RESEARCH PAPER

Elasto-inertial particle focusing in 3D-printed microchannels with unconventional cross sections

Wenlai Tang[1,2] · Ning Fan[1] · Jiquan Yang[1,2] · Zongan Li[1] · Liya Zhu[1] · Di Jiang[3] · Jianping Shi[1] · Nan Xiang[4]

Abstract

In this paper, elasto-inertial particle focusing in 3D-printed microchannels with unconventional cross sections was studied. A novel 3D-printed mold-removal method was proposed to fabricate the microchannels. By modifying the orifice shape of the extrusion nozzle, the microchannel molds with arbitrary cross sections could be printed using an easily accessible fused deposition modeling (FDM) printer. After the routine PDMS casting procedure, the channel molds were dissolved to produce all-PDMS microfluidic chips, thereby eliminating the complex bonding process. The mechanisms of elasto-inertial focusing in the semielliptical and triangular microchannels were explored by comparing the particle migrations in 0.3 wt% HA solution and PBS solution, and the effects of flow rate on particle focusing position and focusing width were also investigated. We found that the single-line particle focusing in the triangular microchannel was more stable and closer to the channel bottom than that in the semielliptical microchannel, which is of great value to improve the detection sensitivity of microfluidic impedance cytometer with coplanar electrodes fabricated on the channel bottom.

Keywords Elasto-inertial focusing · 3D printing · Particle migration · Unconventional cross section · Microfluidics

✉ Jianping Shi
jpshi@njnu.edu.cn

✉ Nan Xiang
nan.xiang@seu.edu.cn

1   School of Electrical and Automation Engineering, Jiangsu Key Laboratory of 3D Printing Equipment and Manufacturing, Nanjing Normal University, 210023 Nanjing, People's Republic of China

2   Nanjing Institute of Intelligent High-end Equipment Industry Co., Ltd, Nanjing, People's Republic of China

3   School of Mechanical and Electronic Engineering, Nanjing Forestry University, Nanjing, People's Republic of China

4   School of Mechanical Engineering, Jiangsu Key Laboratory for Design and Manufacture of Micro-Nano Biomedical Instruments, Southeast University, 211189 Nanjing, People's Republic of China

1 Introduction

Particle manipulation and control in microchannels have recently attracted extensive attention in biological, medical, chemical and environmental fields, due to the numerous advantages of high accuracy, high throughput, low cost and less sample consumption (Wu et al. 2017; Yan et al. 2017). According to their operating principles, the particle manipulating technologies can be categorized as active or passive methods. The active particle manipulations rely on the external forces induced by magnetic (Cho et al. 2017; Zhao et al. 2017), optical (Wang et al. 2011), acoustic (Li et al. 2015; Wang et al. 2018) and electric fields (Sun et al. 2012; Waheed et al. 2018). Nevertheless, the introduction of external fields increases the complexity of microfluidic systems and thus limits their potential point-of-care testing (POCT) applications. On the contrary, the passive particle manipulating technologies can regulate particle migration behaviors by the intrinsic hydrodynamic interactions between microfluid and microchannel structure (Kim et al. 2013; Lu and Xuan 2015; Ranjan et al. 2014).

As a representative of passive technologies, inertial microfluidics has been extensively used for particle ordering, focusing and separation (Di Carlo 2009; Zhang et al. 2016a,

b), due to the characteristics of easy operation and simple microchannel structure. However, the inertial manipulating methods are normally performed in Newtonian fluids such as PBS solution or NaCl solution. Given the fact that many ubiquitous biological fluids including blood, cytoplasm, saliva and semen are non-Newtonian fluids, it is meaningful to study the particle migration behaviors in non-Newtonian fluid flows (Yuan et al. 2018). The non-Newtonian fluids can be prepared by dissolving long-chain molecules in a Newtonian medium, inducing strong viscoelastic effects on particle migration. Compared with inertial focusing in a Newtonian fluid, true 3D particle focusing can be easily realized in simple straight channels in a viscoelastic non-Newtonian fluid (Yang et al. 2011), due to the coupling of inertial effect and viscoelastic effect (i.e., elasto-inertial focusing).

Various microchannel structures, including straight cylindrical channels (Kang et al. 2013; Seo et al. 2014), straight rectangular channels (Del Giudice et al. 2015; Seo et al. 2014a, b), straight channels with side wells (Cha et al. 2014; Yuan et al. 2015) and spiral channels (Lee et al. 2013; Xiang et al. 2016), were proposed for inducing inertial forces, elastic forces and Dean drag forces to perform elasto-inertial particle focusing. Over the past decade, the elasto-inertial focusing technique has been widely employed for particle/cell alignment (Go et al. 2017; Xiang et al. 2018), separation(Liu et al. 2017; Zhang et al. 2016), deformability measurement (Cha et al. 2012; Kim et al. 2017) and solution exchange(Tian et al. 2017; Yuan et al. 2016). However, due to the single-layer processing limitation of the classical soft lithography technique, the mechanism exploration and functional application of elasto-inertial microfluidics are mainly focused on the microchannels with rectangular cross section.

In recent years, researchers have attempted to fabricate non-rectangular microchannels by combining various mold fabrication techniques with conventional PDMS casting procedure. For instance, Warkiani et al. (2014) and Mukherjee et al. (2019) have, respectively, fabricated trapezoid and triangular channel molds by micro-milling a PMMA sheet. Kim et al. (2016) have fabricated semicircular channel molds by reflowing rectangular photoresist and triangular channel molds by anisotropic etching Si wafer. To simplify the channel fabrication, the same group (Kim et al. 2018) also reported a straightforward scribing method to obtain the triangular channel molds. Although microchannels with specified cross sections have been successfully fabricated using the above methods, a general technique to fabricate a wide range of cross-sectional shapes is still lacking. Very recently, particle inertial focusing in triangular and semicircular microchannels has been extensively investigated, and the results show that the non-rectangular microchannels have unique mapping of focusing positions (Kim et al. 2018, 2016; Mukherjee et al. 2019). Nevertheless, to our best knowledge, the elasto-inertial focusing in the microchannels with unconventional cross sections has not been reported up to now.

Herein, we studied the elasto-inertial particle focusing behaviors in semielliptical and triangular microchannels. A novel 3D-printed mold-removal method was proposed to fabricate microchannels with different cross sections. The microchannel molds were printed by using the extrusion nozzles with modified orifice shapes to replace the conventional photolithography technique. All-PDMS microfluidic chips were produced by dissolving the channel molds embedded in cured PDMS to eliminate the complex bonding process. The particle migrations in HA solution and PBS solution were compared to explore the mechanisms of elasto-inertial focusing in the semielliptical and triangular microchannels. Then, the effects of flow rate on particle focusing position and focusing width were also investigated for different cross-sectional microchannels. The results show that, the single-line particle focusing was formed closer to the channel bottom in the semielliptical and triangular microchannels than those in the square and circular ones over a wide range of flow rates, which may serve as a promising pretreatment for microfluidic flow cytometry.

2 Materials and methods

2.1 Microchannel design and fabrication

Straight microchannels with semielliptical and triangular cross sections were designed to be 6 cm long, with a width of 100 μm and a height of 100 μm. The conventional square and circular microchannels with the same dimensions were also designed for comparison. The microchannels were conveniently fabricated using a novel 3D-printed mold-removal method, which consists of extrusion nozzle modifying, ABS mold printing, PDMS casting and sacrificial mold removing, as shown in Fig. 1. The low-cost and commercially available FDM 3D desktop printer (HOFI X1, Nanjing Baoyan Automation Co., Ltd.) is the only main equipment required for the fabrication of different cross-sectional microchannels.

To extrude ABS filaments (microchannel molds) with the desired cross sections, off-the-shelf stainless-steel nozzles were modified by replacing their tips with orificed stainless steel pieces. To be more specific, the tips of the off-the-shelf nozzles were turned by a lathe to expose their circular cross sections with a diameter of about 4 mm. The shaped orifices were then drilled in the circular stainless steel pieces with a thickness of 100 μm and a diameter of 4 mm, by cutting along the contours of the designed channel cross sections with a picosecond laser cutting machine (QS-PICOUV, Jiangyin Deli Laser Solutions Co., Ltd.). Finally, the processed stainless steel pieces were welded

Fig. 1 Fabrication process of the microchannel with unconventional cross section by using the 3D-printed mold-removal method
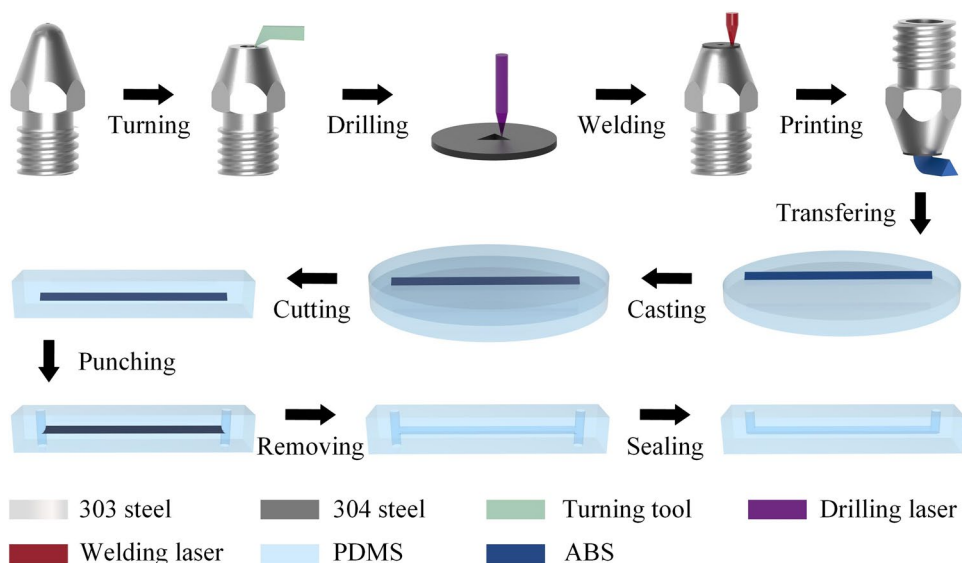
to the top of the cut nozzles with a fiber laser continuous welding machine (YF-FW300, Suzhou Yingfei Laser Technology Co., Ltd.).

The ABS microchannel molds were printed by extruding 1.75 mm ABS filament at 230 °C through the modified nozzles with various shaped orifices. Due to the thermoplasticity of ABS plastics, the printed microchannel molds possess approximately the same cross sections as the orifices in the modified nozzles. Compared with the conventional techniques, the ABS 3D printing with the modified nozzles can fabricate the microchannel molds with different cross sections in an extremely simple and cheap way. After obtaining the ABS molds, the routine PDMS casting procedure was conducted. Specifically, the obtained channel molds were transferred to a 5 mm-thick PDMS block, which was freshly cured in a plastic Petri dish (100 mm). A degassed mixture of PDMS prepolymer and curing agent (Sylgard 184, Dow Corning) with 10:1 mass ratio was then poured above the ABS molds, covering another 5 mm-thick PDMS. After curing in an oven at 80 °C for 2 h, the PDMS block was peeled from the Petri dish and cut into the desired pieces (10 mm wide, 70 mm long). Next, the chip-to-world ports were carefully punched through the two ends of the ABS molds. After that, the PDMS pieces were immersed in acetone and ultrasonically cleaned to remove the ABS sacrificial molds, followed by rinsing in deionized water and drying with nitrogen. To observe the particle focusing behaviors in microchannels from side view, some uncured PDMS was applied and cured on the cut sides of the microfluidic chips to improve the optical imaging quality. Finally, the uncured PDMS was also injected into the bottom half of the punched ports and then cured for the chip sealing, creating all-PDMS microfluidic chips without any additional bonding process.

2.2 Sample preparation and experimental setup

Hyaluronic acid (HA) solution was chose as the viscoelastic medium for suspending particles, due to its biocompatibility and capacity to focus particles over a wide range of flow rates (Lim et al. 2014). The HA solution was prepared by dissolving HA powders (M_w = 265 kDa, Future Industrial Shanghai Co., Ltd) in phosphate-buffered saline (PBS, PH = 7.4, Sigma-Aldrich). To perform elasto-inertial particle focusing, 0.3 wt% HA solution was prepared as it exhibits strong viscoelastic effects. The prepared solution was heated at 80 °C for 24 h and gently shaken several times to ensure the complete dissolution of HA powders. Fluorescent polystyrene particles with diameter of 15 μm were purchased from Huge Biotechnology and dispersed in the prepared HA solution at a very low concentration. Therefore, the interactions between particles can be safely ignored when analyzing the particle focusing behaviors. Before the experiments, Tween 20 (Sigma–Aldrich) was uniformly mixed into the particle suspension (0.5% v/v) by gently shaking to prevent the particles from aggregating and adhering to the microchannel walls.

To observe the particle migrations in the microchannel, the fabricated microfluidic chip was placed on a glass slide and then mounted onto the stage of an inverted fluorescence microscope (IX 71, Olympus). The side view observation of the microchannel can be easily realized by laterally rotating the microfluidic chip with an angle of 90°. The inlet and outlet ports of the microfluidic chip were, respectively, connected to a 10 mL syringe and a 10 mL centrifuge tube via

PTFE tubings. The syringe filled with the prepared particle suspension was loaded onto a precise syringe pump (KDS 270, KD Scientific) for steadily driving the flows. The centrifuge tube was used to collect the particles which flowed through the microfluidic chip. Before every experiment, the microchannel was flushed with PBS solutions for 10 min to remove the dirt and debris.

The particle motions in microchannel were recorded and stored as multiple layered images in TIFF files using a CCD camera (Exi Blue, QImaging) with the supporting IMAGE-PRO Express software. To precisely analyze the particle focusing behaviors, the bright-field images and fluorescent images were, respectively, obtained with the exposure times of 10 μs and 600 ms. The obtained images were processed and analyzed using the open-source ImageJ software (version 1.52a, NIH). To prevent the random errors, multiple image frames under the same condition were stacked to obtain the statistical particle distributions in the microchannel. The stacked images were then used to quantitatively analyze the lateral focusing position and focusing width. In this work, the fluorescent intensity profile across the channel width was extracted and fitted with a Gaussian distribution, and the obtained full width at half maximum (FWHM) and peak position were defined as the particle focusing width and position, respectively.

3 Results and discussion

3.1 Fabrication results of the microchannels

Since the orifice contour of the modified nozzle directly determines the cross section of the printed ABS mold, the picosecond laser drilling of the stainless steel pieces is one critical step to achieve the desired microchannel. Figure 2a shows the microscopic images of the fabricated orifices with different shapes in the modified nozzles. It shows that all the designed channel cross sections including square, circle, triangle and semicircle were successfully transferred to the orifices with good edge quality. For the square, triangular and semielliptical orifices, the small transition arcs around the sharp corners were unavoidable, due to the fact that the circular laser spot was used to drill into the stainless steel pieces. During the microchannel mold printing, the transverse flow of ABS polymers in molten state may lead to the bending of the extruded filaments. To solve this problem, the extrusion speed of ABS filaments and the movement speed of working platform were always kept matched, so that the extruded filaments were straightened (Fig. 2b).

After conducting the routine PDMS casting procedure, the ABS molds embedded in the cured PDMS block were removed by dissolving in acetone. Figure 2c shows the cross-sectional images of the microchannels with different sections obtained after removal of the ABS molds. Compared with the orifice contours in extrusion nozzles, there exist some bulges near the centers of straight edges in the cross sections of the PDMS microchannels. It is easy to understand the reasons for this phenomenon. To print the microchannel mold, the molten ABS must be squeezed into the extrusion nozzle. Therefore, the squeezed ABS needs to swell laterally to release the stress immediately after leaving the nozzle, leading to the bulges near the centers of straight edges having weaker boundary constraints. Although the transition arcs around the sharp corners and the bulges near the centers of straight edges are unavoidable, the fabricated microchannels possess cross sections with designed shapes and dimensions.

Fig. 2 Fabrication results of the 3D-printed microchannels with different cross sections. **a** Images of the square, circular, triangular and semielliptical orifices in the modified nozzles. **b** Image of the ABS mold with circular cross section embedded in the cured PDMS. **c** Cross-sectional images of the microchannels obtained after removal of the ABS molds. The scale bar is 100 μm
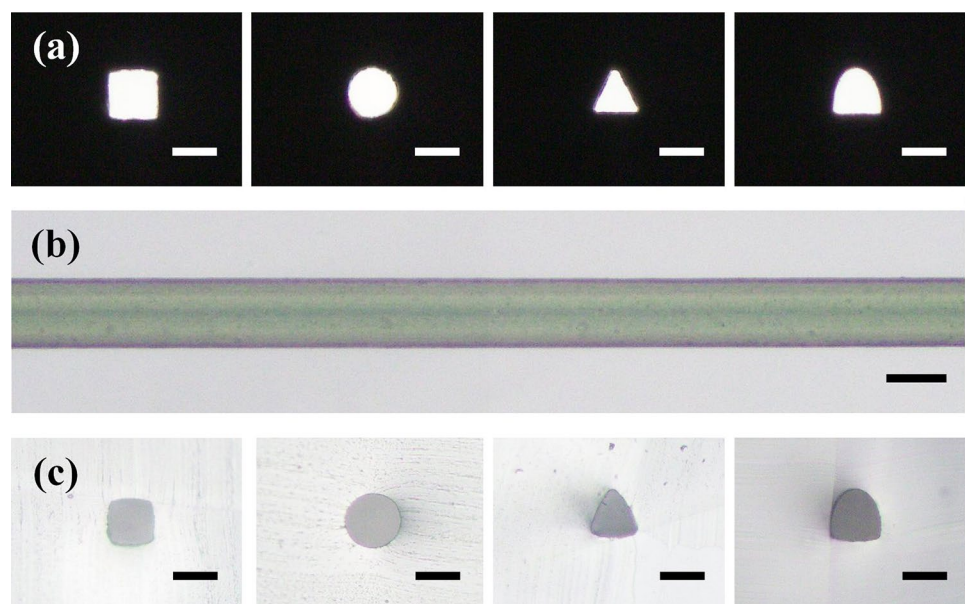
It should be noted that, different from the existing techniques which can only produce microchannel with only one specified section shape, the printed mold-removal method proposed in this work can be used to fabricate microchannels with arbitrary section shapes in a simple and inexpensive way.

3.2 Elasto-inertial focusing in microchannels

The elasto-inertial particle focusing in viscoelastic non-Newtonian fluid flowing through a straight microchannel is a result of competition between transverse inertial lift force and elastic force (Yang et al. 2011). The inertial lift force, which actually includes the shear gradient-induced lift force and wall-induced lift force, can be expressed as $F_L = f_L(\mathrm{Re}_c, x_p)\rho U_m^2 a^4/D_h^2$ (Di Carlo et al. 2008), where f_L is the inertial lift coefficient, Re_c is the channel Reynolds number, x_p is the particle position in channel cross-section, ρ is the fluid density, U_m is the average fluid velocity, a is the particle diameter and D_h is the hydraulic diameter. The channel Reynolds number, defined as $\mathrm{Re}_c = \rho U_m D_h/\mu$ (μ is the dynamic viscosity), can be used to quantify the relative importance of inertial and viscous effects for the given flow condition. The elastic force, which is mainly ascribed to the first normal stress difference N_1 in the viscoelastic fluid, can be estimated as $F_E = f_E a^3 \nabla N_1 = -2f_E a^3 \eta \lambda \nabla \dot{\gamma}^2$ (Lu et al. 2017), where f_E is the elastic lift coefficient, η is the polymeric contribution to solution viscosity, λ is the relaxation time of viscoelastic fluids and $\dot{\gamma}$ is the characteristic shear rate. The viscoelastic effects of a fluid can be quantified using a dimensionless Weissenberg number ($\mathrm{Wi} = \lambda\dot{\gamma} = 2\lambda U_m/D_h$), which describes the ratio of elastic and viscous forces. To directly compare the relative importance of elastic effect to inertial effect, a dimensionless elasticity number is defined as the ratio of Weissenberg number to channel Reynolds number, i.e., $\mathrm{El} = \mathrm{Wi}/\mathrm{Re}_c = 2\lambda\mu/(\rho D_h^2)$ (Lu et al. 2017).

To ensure the elasto-inertial focusing, large polystyrene particles (with a diameter of 15 μm) were dispersed in a high concentrated HA solution (0.3 wt%) to induce both the strong inertial lift force and elastic force. The particle focusing behaviors near the outlet of the semielliptical and triangular microchannels were characterized from both the front and side views. Figure 3a shows the particle focusing images under the fluorescent mode at the driving flow rate of 100 μL/min. The green dotted lines illustrating the channel walls were obtained from the bright-field images under the same experimental conditions. To quantificationally analyze the particle distributions across the channel width, the corresponding normalized fluorescent intensity profiles are plotted in Fig. 3b. The experimental results show that, regardless of microchannel section shapes, there is only one fluorescent stream from both the front and side views, meaning that a true 3D elasto-inertial particle focusing was achieved under the tested condition. From the normalized intensity profiles, we found that the vertical focusing position in the triangular microchannel is lower than that in the semielliptical microchannel, while the horizontal focusing positions are similar for these two microchannels. The detailed reasons will be discussed by combining with the finite element simulation results in the following paragraphs.

To more conveniently explore the mechanism of elasto-inertial particle focusing, the particles were also dispersed in PBS solution to conduct the inertial focusing for comparison. To ensure the inertial focusing, the PBS solution was driven at a high flow rate of 300 μL/min. Under the same experimental condition, the particle distributions in different solutions near the outlet of the semielliptical and triangular microchannels are plotted in Fig. 4a. For directly comparing the particle focusing behaviors from different microchannels and views, the width and height of all microchannels were normalized to 100 μm. From the experimental results of the PBS suspensions, we found that there are three fluorescent peaks from the front view and two fluorescent peaks from the side view, meaning that there exist three inertial focusing positions in both the semielliptical and triangular microchannels. Differing in details, the inertial focusing positions in the triangular microchannel are closer to the channel center on the horizontal plane and lower on the vertical plane.

To better understand the above particle focusing behaviors, the fluid dynamics of non-Newtonian fluids in the semielliptical and triangular microchannels are evaluated by the FEM simulations using COMSOL Multiphysics software, assuming a constant fluid viscosity. The flow velocity and shear rate distributions on the microchannel sections obtained from simulation results at a flow rate of 300 μL/min are demonstrated in Fig. 4b. The black dotted circles representing the inertial focusing positions, the maroon dotted circles representing the elastic focusing positions and the maroon solid circles representing the elasto-inertial focusing positions are also presented. The positions of the black dotted circles and maroon solid circles are determined according to the fluorescent peaks in Fig. 4a.

From the simulation results, we found that the laminar flow in the microchannel results in a radially parabolic velocity profile. Due to the balance between shear gradient-induced lift force and wall-induced lift force, three inertial focusing positions near the centers of the triangular microchannel faces are formed in the PBS solution, which is consistent with the previous report (Kim et al. 2016). However, the inertial particle focusing behaviors in the semielliptical microchannel are different from those in the semicircular microchannel as previously reported; there are three focusing positions near the centers of the semielliptical microchannel faces, while there are only two focusing positions near the centers of the top and bottom channel walls in the semicircular microchannel. In fact, the semielliptical channel

Fig. 3 Particle focusing in 0.3 wt% HA solution flowing through the semielliptical and triangular microchannels at a flow rate of 100 μL/min. **a** Stacked particle focusing images under the dark fluorescent mode. The green dotted lines clearly mark the positions of channel walls. The red and blue lines are plotted across the channel to obtain the fluorescent intensity profiles. **b** Normalized fluorescent intensity profiles illustrating the particle distributions across the channel width (red) and channel height (blue). The scale bar in **a** represents 100 μm. (Color figure online)
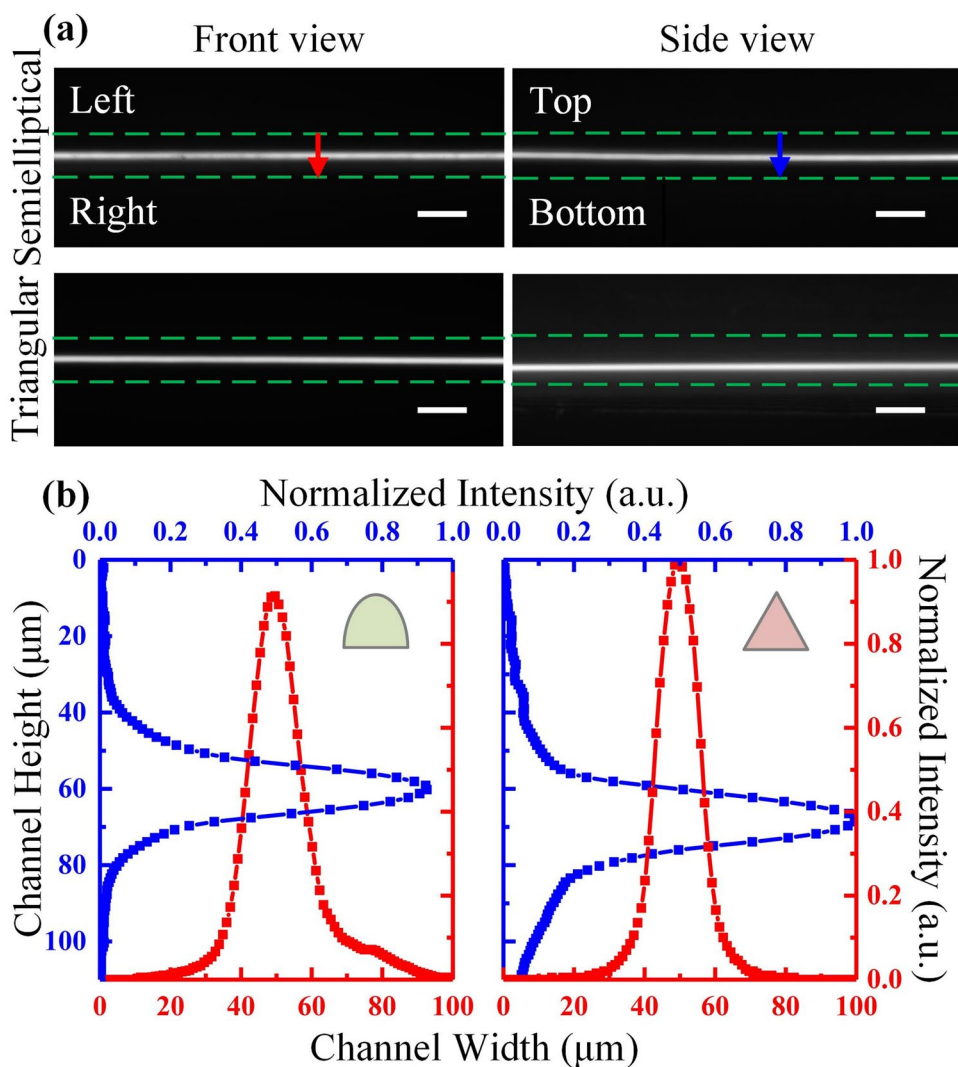
designed in this work holds twice the height of the semicircular one, making the focusing behaviors in the semielliptical channel similar to those in the triangular channels, while the focusing behaviors in the semicircular channel are similar to those in the low-aspect-ratio rectangular channels (Zhang et al. 2016a, b). We can also see that the flow velocity distributions in the triangular channel are more concentrated downward than those in the semielliptical one, resulting in the particles moving closer to the channel center horizontally and to the channel bottom vertically.

Considering only the elastic effects in non-Newtonian fluid, the particles will be focused at the center and the two corners in the semielliptical microchannel, but at the center and the three corners in the triangular microchannel, where the shear rates are smallest (Fig. 4b). However, only one focusing position was experimentally observed in the 0.3 wt% HA solution for both the semielliptical and triangular microchannels. When flowing in the HA solution, the particles are influenced by both the inertial lift force and elastic force. Under the effects of elastic force, the three inertial focusing positions become unstable. Meanwhile, the elastically focused particles are pushed away from the corners due to the strong wall-induced lift force. However, the particle alignment along the channel centerline caused by the fluid elasticity is still retained, due to the fact that both the inertial and elastic forces are balanced. This single-line focusing along the centerline is well known as the elasto-inertial focusing. The FEM simulation results show that the flow dynamics are horizontal symmetry, leading to the focusing positions being horizontally centered for both the semielliptical and triangular channels. However, the vertical focusing position in the triangular microchannel is closer to the channel bottom than that of the semielliptical one, because the zone of smallest shear rate in the triangular microchannel is much lower.
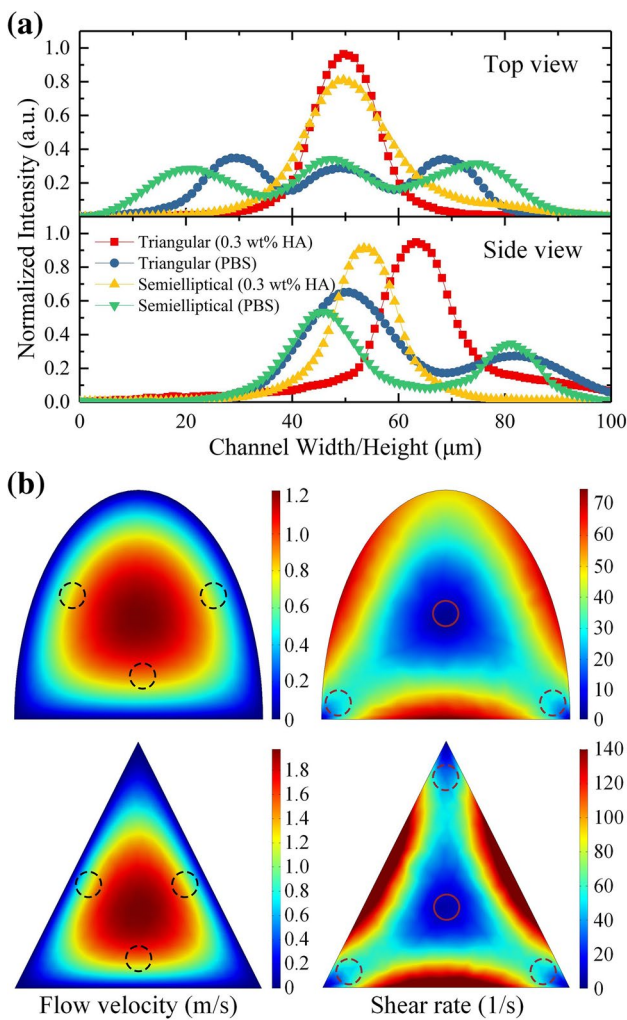
(a)

(b)

Flow velocity (m/s)   Shear rate (1/s)

Fig. 4 Elasto-inertial particle focusing mechanism in the semielliptical and triangular microchannels. **a** Normalized fluorescent intensity profiles illustrating the particle distributions in different suspensions at a flow rate of 300 μL/min. **b** Comsol simulations showing the flow velocity and shear rate distributions of non-Newtonian fluid flowing in the semielliptical and triangular microchannel under the same experimental condition as **a**. The black dotted circles represent the inertial focusing positions, the maroon dotted circles represent the elastic focusing positions and the maroon solid circles represent the elasto-inertial focusing positions. (Color figure online)

3.3 Effects of flow rate

To investigate the effects of flow rate on the elasto-inertial focusing, the particles suspended in HA solution were injected over the driving flow rates from 1 to 300 μL/min for both the semielliptical and triangular microchannels. The same experiments were also conducted in the microchannels with square and circular cross sections for comparison. To better compare the particle focusing behaviors in different microchannels, all the channel widths and heights were normalized to 100 μm. The normalized fluorescent intensity

profiles illustrating the particle distributions in the semielliptical and triangular microchannels at different flow rates are shown in Fig. 5a, b. The results show that a few particles were focused around the corner of the semielliptical channel at the lowest flow rate (1 μL/min), due to the wall-induced lift force becoming weaker. However, the three-dimensional focusing near the channel center was observed under all the other experimental conditions in both the semielliptical and triangular microchannels, which means that elasto-inertial focusing can be achieved over a wide range of flow rates. It should be noted that, most of the particles were still focused near the semielliptical channel center even at a flow rate of 1 μL/min, due to the strong viscoelastic effects of the high concentrated HA solution. Therefore, very few particles around the channel corner were randomly recorded in one image sequence, leading to the results that only one small intensity peak can be seen from the front view in Fig. 5a.

Considering the flow rates from 5 to 300 μL/min, where the 3D particle focusing was formed, the focusing widths (the FWHMs of the fluorescent intensity profiles) and focusing positions (the peaks positions of the fluorescent intensity profiles) were plotted as a function of flow rate (Fig. 5c). To better understand the effects of channel sections on particle focusing behaviors, four microchannels with different cross sections including square, circle, triangle and semiellipse were considered. From the measured focusing positions, we found that all the particles were focused near the center of the microchannel under each experimental condition. The blockage ratio $\beta = a/D_h$ is an important parameter that determines the elasto-inertial particle focusing behaviors (Yuan et al. 2017). Regardless of the initial positions, particles with blockage ratio less than 0.25 will be pushed toward the centerline of the channel, while particles with blockage ratio greater than 0.25 will migrate to the side walls. For the 15 μm particles used in this work, the blockage ratios in the square, circular, semielliptical and triangular microchannels are 0.15, 0.15, 0.17 and 0.24, respectively, all below the critical blockage ratio $\beta = 0.25$. Therefore, although there are some fluctuations, the particle focusing positions remain stable near the channel centerline under all the tested flow rates for each microchannel. In addition, the curves of focusing width illustrated in Fig. 5c clearly show that the particles flowing in the semielliptical and triangular microchannels were focused closer to the channel bottom than those in the square and circular microchannels.

In terms of the measured focusing widths, the semielliptical microchannel has wider focusing width than triangular microchannel on the horizontal plane, while the opposite is true for the vertical plane. We can also see that the particles flowing in the square and circular microchannels could be focused into a much narrower stream as compared with that in the semielliptical and triangular microchannels at all the tested flow rates. The particle focusing in the circular
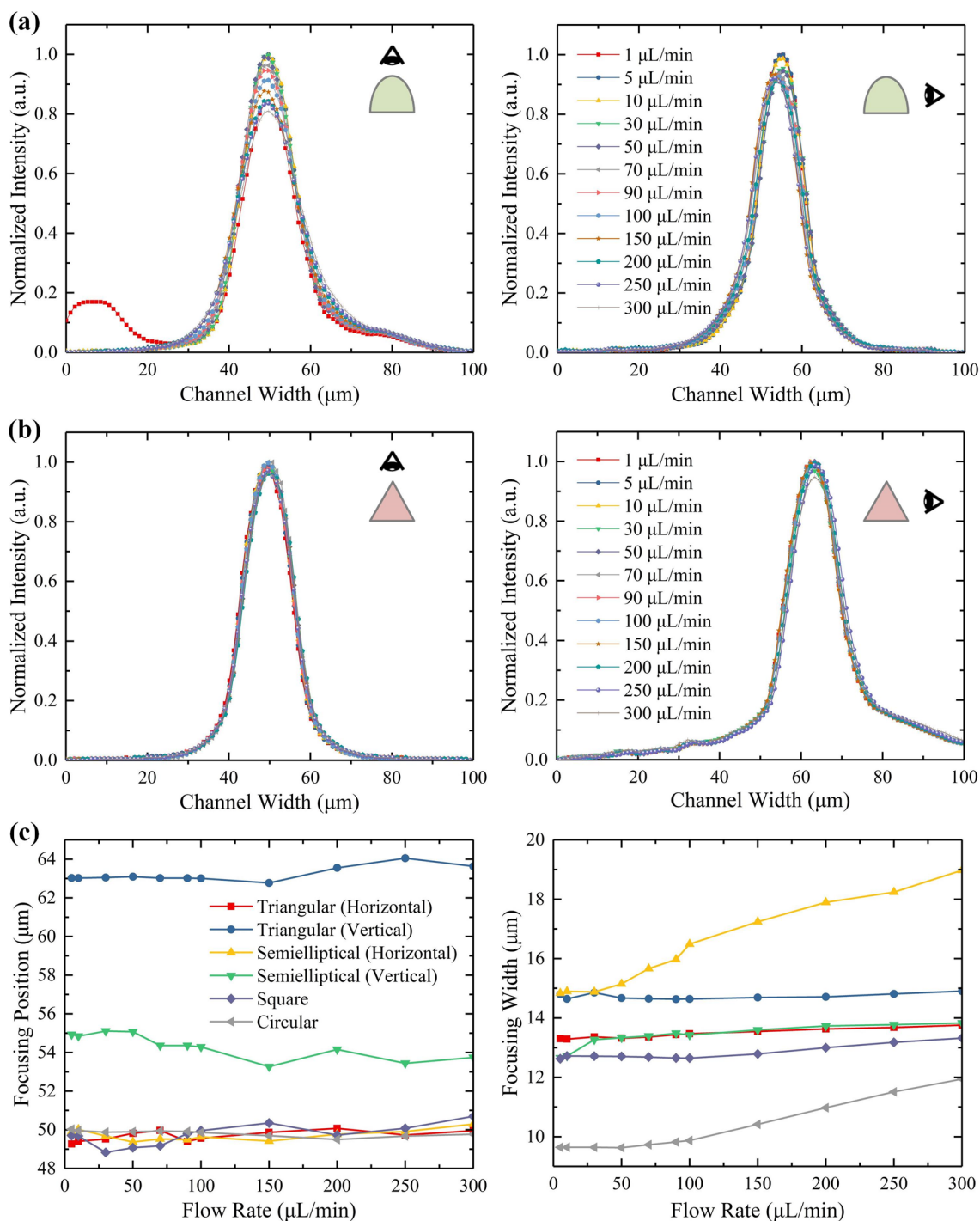
Fig. 5 Effects of flow rate on the elasto-inertial particle focusing in the microchannels with semielliptical and triangular cross section. **a** Normalized fluorescent intensity profiles illustrating the particle distributions in the semielliptical microchannel at the flow rates from 1 to 300 μL/min. **b** Normalized fluorescent intensity profiles illustrat- ing the particle distributions in the triangular microchannel under the same experimental conditions as **a**. **c** Measured particle focusing positions (the peak positions of the intensity profiles) and focusing widths (the FWHMs of the intensity profiles) in different cross-sec- tional microchannels as a function of flow rate

microchannel and semielliptical microchannel from the front view becomes looser with increasing flow rate in the cur- rent flow regime, while the focusing widths remain stable in

the square microchannel, triangular microchannel and sem- ielliptical microchannel from the side view. Based on the above discussions, we found that the elasto-inertial particle

focusing in the triangular microchannel is more stable and closer to the channel bottom than that in the semielliptical microchannel, which is promising for improving the detection sensitivity of the microfluidic impedance cytometer with coplanar electrodes (Yang et al. 2018).

4 Conclusions

In this work, a novel 3D-printed mold-removal method was proposed to fabricate the microchannels with semielliptical, triangular, square and circular sections in a low-cost, convenient and efficient way. Microchannels with other cross sections can also be produced with this method by just changing the orifice shapes in the printer nozzles. In addition, 3D microchannels with arbitrary section shapes are expected to be fabricated when complementing a multi-degree of freedom (DOF) motion platform. The elasto-inertial particle focusing behaviors in the microchannels with unconventional cross sections were investigated. It is found that 3D single-line focusing was achieved in both the semielliptical and triangular microchannels over a wide range of flow rates. Compared with the well-known square and circular microchannels, the particles were focused closer to the channel bottom in the semielliptical and triangular microchannels. This lower single-line particle focusing would be valuable for the downstream microfluidic impedance cytometer with detection electrodes fabricated on the channel bottom.

References

Cha S, Shin T, Lee SS, Shim W, Lee G, Lee SJ, Kim Y, Kim JM (2012) Cell stretching measurement utilizing viscoelastic particle focusing. Anal Chem 84:10471–10477

Cha S, Kang K, You JB, Im SG, Kim Y, Kim JM (2014) Hoop stress-assisted three-dimensional particle focusing under viscoelastic flow. Rheol Acta 53:927–933

Cho H, Kim J, Jeon C-W, Han K-H (2017) A disposable microfluidic device with a reusable magnetophoretic functional substrate for isolation of circulating tumor cells. Lab Chip 17:4113–4123

Del Giudice F, D'Avino G, Greco F, Netti PA, Maffettone PL (2015) Effect of fluid rheology on particle migration in a square-shaped microchannel. Microfluid Nanofluid 19:95–104

Di Carlo D (2009) Inertial microfluidics. Lab Chip 9:3038–3046

Di Carlo D, Edd JF, Irimia D, Tompkins RG, Toner M (2008) Equilibrium separation and filtration of particles using differential inertial focusing. Anal Chem 80:2204–2211

Go T, Byeon H, Lee SJ (2017) Focusing and alignment of erythrocytes in a viscoelastic medium. Sci Rep 7:41162

Kang K, Lee SS, Hyun K, Lee SJ, Kim JM (2013) DNA-based highly tunable particle focuser. Nat Commun 4:2567

Kim MS, Kim J, Lee W, Cho S-J, Oh J-M, Lee J-Y, Baek S, Kim YJ, Sim TS, Lee HJ, Jung G-E, Kim S-I, Park J-M, Oh JH, Gurel O, Lee SS, Lee J-G (2013) A trachea-inspired bifurcated microfilter capturing viable circulating tumor cells via altered biophysical properties as measured by atomic force microscopy. Small 9:3103–3110

Kim J, Lee J, Wu C, Nam S, Di Carlo D, Lee W (2016) Inertial focusing in non-rectangular cross-section microchannels and manipulation of accessible focusing positions. Lab Chip 16:992–1001

Kim J, Kim JY, Kim Y, Lee SJ, Kim JM (2017) Shape measurement of ellipsoidal particles in a cross-slot microchannel utilizing viscoelastic particle focusing. Anal Chem 89:8662–8666

Kim J-a, Lee J-R, Je T-J, Jeon E-c, Lee W (2018) Size-dependent inertial focusing position shift and particle separations in triangular microchannels. Anal Chem 90:1827–1835

Lee DJ, Brenner H, Youn JR, Song YS (2013) Multiplex particle focusing via hydrodynamic force in viscoelastic fluids. Sci Rep 3:3258

Li P, Mao Z, Peng Z, Zhou L, Chen Y, Huang P-H, Truica CI, Drabick JJ, El-Deiry WS, Dao M, Suresh S, Huang TJ (2015) Acoustic separation of circulating tumor cells. Proc Natl Acad Sci USA 112:4970–4975

Lim EJ, Ober TJ, Edd JF, Desai SP, Neal D, Bong KW, Doyle PS, McKinley GH, Toner M (2014) Inertio-elastic focusing of bioparticles in microchannels at high throughput. Nat Commun 5:4120–4120

Liu C, Guo JY, Tian F, Yang N, Yan FS, Ding YP, Wei JY, Hu GQ, Nie GJ, Sun JS (2017) Field-free isolation of exosomes from extracellular vesicles by microfluidic viscoelastic flows. Acs Nano 11:6968–6976

Lu XY, Xuan XC (2015) Continuous microfluidic particle separation via elasto-inertial pinched flow fractionation. Anal Chem 87:6389–6396

Lu XY, Liu C, Hu GQ, Xuan XC (2017) Particle manipulations in non-Newtonian microfluidics: A review. J Colloid Interface Sci 500:182–201

Mukherjee P, Wang X, Zhou J, Papautsky I (2019) Single stream inertial focusing in low aspect-ratio triangular microchannels. Lab Chip 19:147–157

Ranjan S, Zeming KK, Jureen R, Fisher D, Zhang Y (2014) DLD pillar shape design for efficient separation of spherical and non-spherical bioparticles. Lab Chip 14:4250–4262

Seo KW, Ha YR, Lee SJ (2014a) Vertical focusing and cell ordering in a microchannel via viscoelasticity: Applications for cell monitoring using a digital holographic microscopy. Appl Phys Lett 104:213702

Seo KW, Byeon HJ, Huh HK, Lee SJ (2014b) Particle migration and single-line particle focusing in microscale pipe flow of viscoelastic fluids. RSC Adv 4:3512–3520

Sun JS, Gao YD, Isaacs RJ, Boelte KC, Lin PC, Boczko EM, Li DY (2012) Simultaneous on-chip DC dielectrophoretic cell separation and quantitative separation performance characterization. Anal Chem 84:2017–2024

Tian F, Zhang W, Cai L, Li S, Hu G, Cong Y, Liu C, Li T, Sun J (2017) Microfluidic co-flow of Newtonian and viscoelastic fluids for high-resolution separation of microparticles. Lab Chip 17:3078–3085

Waheed W, Alazzam A, Mathew B, Christoforou N, Abu-Nada E (2018) Lateral fluid flow fractionation using dielectrophoresis (LFFF-DEP) for size-independent, label-free isolation of circulating tumor cells. J Chromatogr B 1087:133–137

Wang X, Chen S, Kong M, Wang Z, Costa KD, Li RA, Sun D (2011) Enhanced cell sorting and manipulation with combined

optical tweezer and microfluidic chip technologies. Lab Chip 11:3656–3662

Wang KY, Zhou W, Lin ZG, Cai FY, Li F, Wu JR, Meng L, Niu LL, Zheng HR (2018) Sorting of tumour cells in a microfluidic device by multi-stage surface acoustic waves. Sensor Actuat B-Chem 258:1174–1183

Warkiani ME, Guan G, Luan KB, Lee WC, Bhagat AAS, Kant Chaudhuri P, Tan DS-W, Lim WT, Lee SC, Chen PCY, Lim CT, Han J (2014) Slanted spiral microfluidics for the ultra-fast, label-free isolation of circulating tumor cells. Lab Chip 14:128–137

Wu J, Chen Q, Lin J-M (2017) Microfluidic technologies in cell isolation and analysis for biomedical applications. Analyst 142:421–441

Xiang N, Zhang X, Dai Q, Cheng J, Chen K, Ni Z (2016) Fundamentals of elasto-inertial particle focusing in curved microfluidic channels. Lab Chip 16:2626–2635

Xiang N, Ni ZH, Yi H (2018) Concentration-controlled particle focusing in spiral elasto-inertial microfluidic devices. Electrophoresis 39:417–424

Yan S, Zhang J, Yuan D, Li WH (2017) Hybrid microfluidics combined with active and passive approaches for continuous cell separation. Electrophoresis 38:238–249

Yang S, Kim JY, Lee SJ, Lee SS, Kim JM (2011) Sheathless elasto-inertial particle focusing and continuous separation in a straight rectangular microchannel. Lab Chip 11:266–273

Yang RJ, Fu LM, Hou HH (2018) Review and perspectives on microfluidic flow cytometers. Sensor Actuat B-Chem 266:26–45

Yuan D, Zhang J, Yan S, Pan C, Alici G, Nguyen NT, Li WH (2015) Dean-flow-coupled elasto-inertial three-dimensional particle focusing under viscoelastic flow in a straight channel with asymmetrical expansion–contraction cavity arrays. Biomicrofluidics 9:044108

Yuan D, Zhang J, Yan S, Peng G, Zhao Q, Alici G, Du H, Li W (2016) Investigation of particle lateral migration in sample-sheath flow of viscoelastic fluid and Newtonian fluid. Electrophoresis 37:2147–2155

Yuan D, Tan SH, Zhao Q, Yan S, Sluyter R, Nguyen NT, Zhang J, Li W (2017) Sheathless Dean-flow-coupled elasto-inertial particle focusing and separation in viscoelastic fluid. RSC Adv 7:3461–3469

Yuan D, Zhao Q, Yan S, Tang S-Y, Alici G, Zhang J, Li W (2018) Recent progress of particle migration in viscoelastic fluids. Lab Chip 18:551–567

Zhang J, Yan S, Yuan D, Alici G, Nguyen NT, Warkiani ME, Li WH (2016a) Fundamentals and applications of inertial microfluidics: a review. Lab Chip 16:10–34

Zhang J, Yan S, Yuan D, Zhao Q, Tan SH, Nguyen N-T, Li W (2016b) A novel viscoelastic-based ferrofluid for continuous sheathless microfluidic separation of nonmagnetic microparticles. Lab Chip 16:3947–3956

Zhao WJ, Cheng R, Lim SH, Miller JR, Zhang WZ, Tang W, Xie J, Mao LD (2017) Biocompatible and label-free separation of cancer cells from cell culture lines from white blood cells in ferrofluids. Lab Chip 17:2243–2255